Communications Chemistry

https://doi.org/10.1038/s42004-025-01870-y

Article in Press

Low-energy glycine formation and spectral masking in star-forming regions

Received: 8 October 2025

Accepted: 15 December 2025

Cite this article as: Mates-Torres, E., Rimola, A. Low-energy glycine formation and spectral masking in star-forming regions. *Commun Chem* (2025). https://doi.org/10.1038/s42004-025-01870-y

Eric Mates-Torres & Albert Rimola

Low-energy glycine formation and spectral masking in star-forming regions

Eric Mates-Torres[1]*, Albert Rimola[1,2]*

[1]Departament de Química, Universitat Autònoma de Barcelona, 08193 Bellaterra, Catalonia, Spain
[2]Accademia delle Scienze di Torino, Via Maria Vittoria, 3, 10123 Torino, Italy

*Correspondence e-mail: eric.mates@uab.cat, albert.rimola@uab.cat

Abstract

The presence of amino acids in comets and meteorites has long suggested that prebiotic molecules may have formed in space and contributed to the origins of life on Earth. Glycine, the simplest amino acid, has been identified in several extraterrestrial environments, although its detection in the interstellar medium, including prestellar cores and protostellar regions, remains elusive. Here, we investigate a novel catalytic pathway for glycine formation on silicate grains during relatively warm (>150 K) stages of star formation. Using atomistic simulations, the feasibility of a Strecker-type synthesis and a direct neutral mechanism involving reactivity between formaldehyde, carbon monoxide and ammonia on forsterite surfaces, the major constituent of interstellar dust, is assessed. Results show that the Strecker pathway is limited by high activation barriers, whereas the proposed direct mechanism proceeds through low-energy surface-stabilized intermediates leading to spontaneous formation of glycine in a single-barrier exoergic process. Additionally, glycine strongly adsorbs onto the mineral surface and is unlikely to desorb under warm conditions. A vibrational analysis reveals that glycine formed through this pathway exhibits spectrally distinct features, including suppression and shifting of characteristic bands, which may account for its persistent non-detection in astronomical observations.

Introduction

Amino acids are key biomolecules in the development of early life on Earth. Its simplest constituent, glycine (Gly, NH_2CH_2COOH), has been routinely found in almost racemic enantiomeric ratios in meteorites and, recently, in returned samples from the Ryugu asteroid.[1–3] Gly has also been detected in returned coma samples of the 81P/Wild 2 comet[4,5] and in the coma of 67P/Churyumov-Gerasimenko by in-situ mass spectroscopy.[6] Numerous efforts have been undertaken to identify Gly in the interstellar medium (ISM), but its unambiguous detection remains elusive,[7–9] and only its more stable isomers have been observed.[10,11]

Despite unsuccessful attempts to find amino acids in star-forming environments,[12–14] these regions are highly promising for the presence of Gly, given that their rich molecular compositions closely match those observed in cometary atmospheres.[15,16] Chemical evolution in these regions goes through three stages, namely cold, warm-up and hot-core.[17,18] In the cold stage (~10 K), so-called zeroth-generation molecules such as methane (CH_4), methanol (CH_3OH) and ammonia (NH_3) are formed mainly through hydrogenations occurring on the water-dominated ice mantles.[19] In the warm-up phase, as temperatures rise to 100–300 K, thermal processing and increased radical mobility allow for the synthesis of more complex, first-generation species, among them interstellar complex organic molecules (iCOMs), such as formamide (NH_2CHO) acetaldehyde (CH_3CHO) or methylformate (CH_3OCHO) through gas-phase reactions or grain surface-mediated radical-radical and radical-neutral reactions on the ice mantle.[20] Surrounding ignited young stars in the hot-core phase, higher temperatures yield complete evaporation of the ices and of trapped iCOMs within a radius from the protoplanetary disk (the "snow-line").[14] This phenomenon allows for more complex chemistry occurring in the gas-phase, where sublimated neutral molecules may react to form large and complex species in energy barrier-bearing and even potentially endergonic processes. Thus, gas-phase reaction routes for the formation of Gly in these scenarios have been proposed, mainly through quantum mechanical methods, involving radical-radical couplings,[21] interactions between closed-shell species and either radicals[22–24] or ions,[25–28] and reactions involving purely neutral molecules.[23,29–33] Many of the proposed reaction mechanisms stem from first-generation molecular species found along the Strecker synthesis (the main multistep route for the formation of amino acids from aldehydes in solution)[34] such as methanimine (CH_2=NH) or aminoacetonitrile (NH_2CH_2CN), and depend on the availability of reactive radical or charged species—which in turn demand energetic processing of stable zeroth-generation molecules—, mostly displaying prohibitively high activation barriers. In turn, the ability of water ice to act as catalyst for this reaction in colder regions of star formation has also been shown, with reactions involving radical and ionized ice and/or reactants,[35,36] concerted three-body processes[37] or displaying relatively large energetic barriers,[38] thus requiring temperatures incompatible with the stability of the ice on the grain.[17] Nonetheless, experimental breakthroughs have demonstrated feasible routes for Gly formation under cold conditions. Notably, Ioppolo et al. showed that Gly can form via barrierless radical-radical recombination (e.g., NH_2CH_2 + HO–CO) on water-rich ices at temperatures as low as 13 K.[39] These ice-dominated pathways are crucial during the early, cold stages of star formation; however, as the system evolves into warmer phases of star formation with higher temperatures, water ice sublimation uncovers a seldom explored scenario, where zeroth- and first-generation species may accrete on the bare silicate surfaces that conform the grain cores, thus potentially undergoing heterogeneous catalysis towards Gly. In

that regard, the adsorption of relevant molecules with prebiotic potential, such as H_2CO,[40] HCN[41,42] and S-bearing species[43,44] has been modelled on silicate surfaces, the main mineral conforming interstellar grains, meteorites and comets.[45,46] Successively, these mineral interfaces have been shown to catalyze biologically relevant processes such as the formose reaction[47,48] or HCN polymerization.[49] Thus, parent body-dominated chemical processes may hold the key to understand the formation of Gly in star forming regions.[50,51]

In this article, we address, for the first time, the role of interstellar mineral interfaces in the formation of Gly from abundant zeroth-generation molecules and its subsequent inclusion in cometary and meteoritic phases using quantum chemical atomistic modelling. The study is structured to contrast two distinct formation paradigms. First, we assess the feasibility of the conventional formation route for Gly in solution, the Strecker synthesis, catalyzed on the parent body, and demonstrate that this route is hindered by high activation barriers. In response to these energetic limitations, we then propose and characterize a novel, direct non-Strecker mechanism involving the reaction of H_2CO, CO, and NH_3. We show that this alternative pathway proceeds through low-energy, surface-stabilized intermediates to yield Gly spontaneously, which we further characterize via vibrational analysis to provide a potential explanation for the molecule's persistent non-detection in astronomical gas-phase observations.

Results and discussion

Bare grain-mediated Strecker synthesis. The Strecker synthesis consists of three steps: i) formation of methanimine ($NHCH_2$) *via* reaction of NH_3 and H_2CO forming first aminomethanol (NH_2CH_2OH) followed by its dehydration, ii) formation of aminonitrile (NH_2CH_2CN) through reaction of $NHCH_2$ and HCN, and iii) acidic hydrolysis of NH_2CH_2CN finally forming Gly. Each of these steps requires multiple proton transfers bearing barriers of up to 31 kcal mol^{-1}, which in solution are facilitated by water solvent molecules.[34] It is important to note that $NHCH_2$ is a well-known interstellar species, first identified in the Sgr B2 hot core,[52] and its high abundance in the Galactic Center[53,54] suggests that inherited chemical complexity could theoretically facilitate the Strecker synthesis, potentially bypassing the initial formation step. Furthermore, reaction networks indicate facile formation of $NHCH_2$,[55] and its precursor NH_2CH_2OH has been found to form readily on interstellar ices.[56] However, to comprehensively assess the potential for a self-sufficient catalytic pathway starting from abundant zeroth-generation precursors, thereby establishing a solid baseline for comparison with alternative proposed mechanisms, our model explicitly assesses the surface-mediated formation of $NHCH_2$ on bare grain silicates.

To better depict the conditions in star forming regions, our model considers mechanisms involving abundant zeroth-generation species that accrete onto

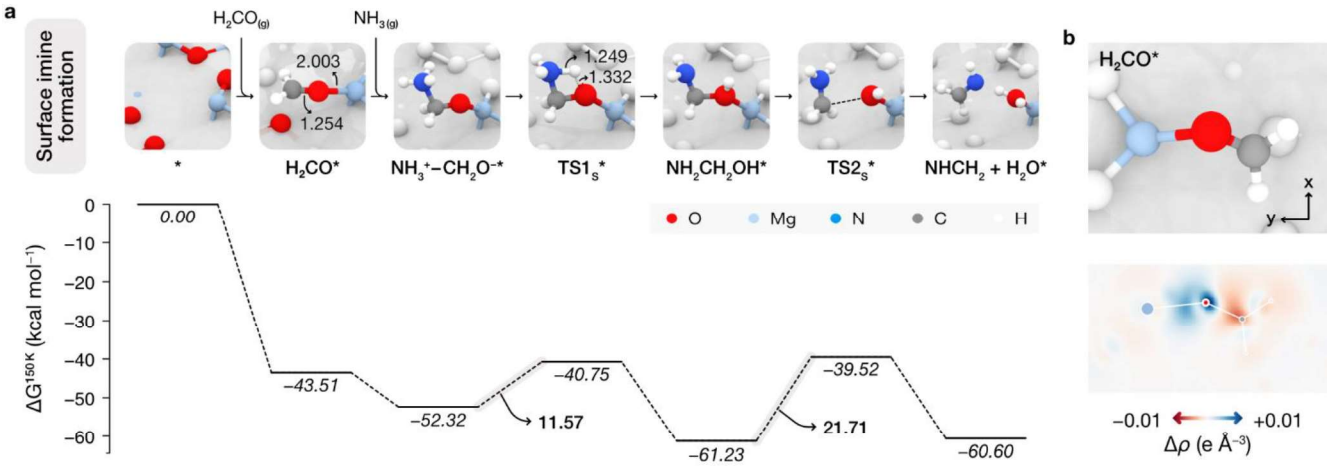

Figure 1. Proposed Strecker-type pathway on Mg_2SiO_4. a, HSE06-D3//PBE-D3-calculated reaction pathway and free energy diagrams at 150 K of imine formation on Mg_2SiO_4(120) adopting a Strecker-type mechanism. A standalone asterisk is used to denote the bare surface, whereas when used alongside a molecular species denotes its adsorbed configuration. Relevant bond distances are depicted in Å on the atomic representations. Atoms belonging to the adsorbate and relevant surface atoms have been colored; the remaining surface atoms have been whitened out for clarity. **b,** On the top panel, top-view representation of the H_2CO molecule adsorbed on the (120) surface of Mg_2SiO_4. On the bottom panel, c-axis averaged charge density differences between the surface and the adsorbed H_2CO molecule. Red and blue regions depict a decrease or increase in charge density upon adsorption, respectively.

the bare grains after ice sublimation, i.e., H_2CO, CO and NH_3. In this scenario, our atomistic structural models mimicking the bare grain surfaces consist of crystalline forsterite (Mg_2SiO_4), an abundant silicate conforming interstellar grains. To model $NHCH_2$ formation, the simulated Strecker pathway (whose results are shown in Figure 1a) begins with the adsorption of H_2CO through its O atom atop an undercoordinated Mg ion of Mg_2SiO_4(120), the most extended termination of forsterite-covering a fraction of 0.331 of the equilibrium shape of forsterite at 0 K-,[44] forming H_2CO^* (an asterisk denotes adsorbed species) with a binding Gibbs energy of 43.51 kcal mol^{-1}. Interestingly, subsequent reaction of H_2CO^* with an incoming NH_3 yields the spontaneous (i.e., exoergic and barrierless) formation of zwitterionic aminomethanol (NH_3^+–CH_2O^{-*}), which can convert into its canonical form, $NH_2CH_2OH^*$, through a proton transfer between both terminal moieties with a barrier of 11.57 kcal mol^{-1} ($TS1_S^*$ of Figure 1a). Cleavage of the C-O bond and subsequent proton-transfer from the NH_2 moiety to the O atom yields $NHCH_2$ formation and an adsorbed water in the active site ($NHCH2+H_2O^*$ of Figure 1) in a slightly endoergic process, requiring an activation barrier of 21.71 kcal mol^{-1} ($TS2_S^*$). At a representative warm region temperature of 150 K, the rate constant arising from the rate limiting step, i.e. the release of $NHCH_2$ from dehydration of $NH_2CH_2OH^*$, is calculated to be 2.31×10^{-6} Myr^{-1}. Thus, based on the simulations of the first step in the Strecker synthesis, our calculations predict a limited catalytic impact of the bare grain surface with respect to the conventional reaction in solution.

Direct glycine formation pathway. Having discarded the possibility of a Strecker-type mechanism catalyzed on the mineral surface, we then turned our attention to potential non-Strecker reaction mechanisms not governed by H-transfers or

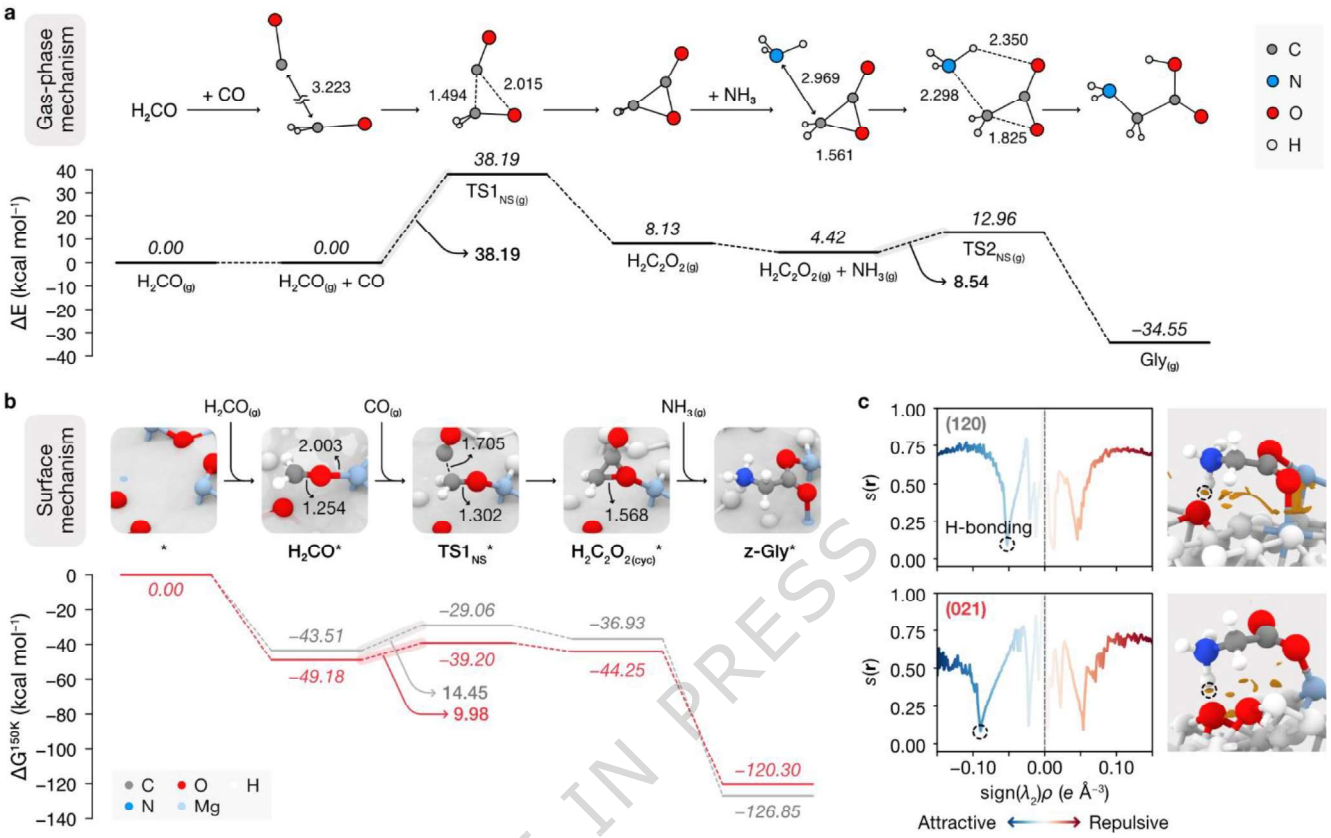

Figure 2. Proposed direct Gly formation on Mg_2SiO_4. a, HSE06-D3//PBE-D3-calculated reaction pathway for the direct non-Strecker formation of Gly from zeroth-generation molecular species in the gas phase. Relevant bond distances are depicted in Å on the atomic representations. **b**, Proposed reaction mechanisms and calculated free energy diagrams at 150 K of the direct and neutral formation of z-Gly on Mg_2SiO_4(120) (gray line) and Mg_2SiO_4(021) (red line). A standalone asterisk is used to denote the bare surface, whereas when used alongside a molecular species denotes its adsorbed configuration. Relevant bond distances are depicted in Å on the atomic representations. Atoms belonging to the adsorbate and relevant surface atoms have been colored; the remaining surface atoms have been whitened out for clarity. **c**, Pseudo-quantitative analysis of the non-covalent interactions governing the adsorption and stabilization of the formed z-Gly* on Mg_2SiO_4(120) (top panels) and Mg_2SiO_4(021) (bottom panels). Side view representations of the isosurfaces displaying regions of non-covalent interaction (with an isovalue of 0.3 e Å^{-3}) are depicted on the right panels. H-bonding regions in the isosurfaces, along with their corresponding peak in the non-covalent interaction plot, are denoted with a dashed circle.

hydrolysis, where the role of water molecules is a requisite. In that regard, our simulations showed that the barrierless combination between the H_2CO* intermediate and NH_3 in the studied Strecker-type pathway is driven by a surface-induced charge polarization of the former. Specifically, a charge density difference analysis of H_2CO* revealed a depletion of electron density around the C atom—and thus an increase of its cationic nature (red area in Figure 1b)—and a consequent increase in the electron density around the O moiety of H_2CO* (blue area in Figure 1b), driven by the strong Lewis acidic nature of the surface Mg atom. In view of these results, we then revisited a direct neutral mechanism proposed by Maeda and Ohno[23] and envisioned a mineral-borne pathway where H_2CO* reacts with ISM-abundant CO

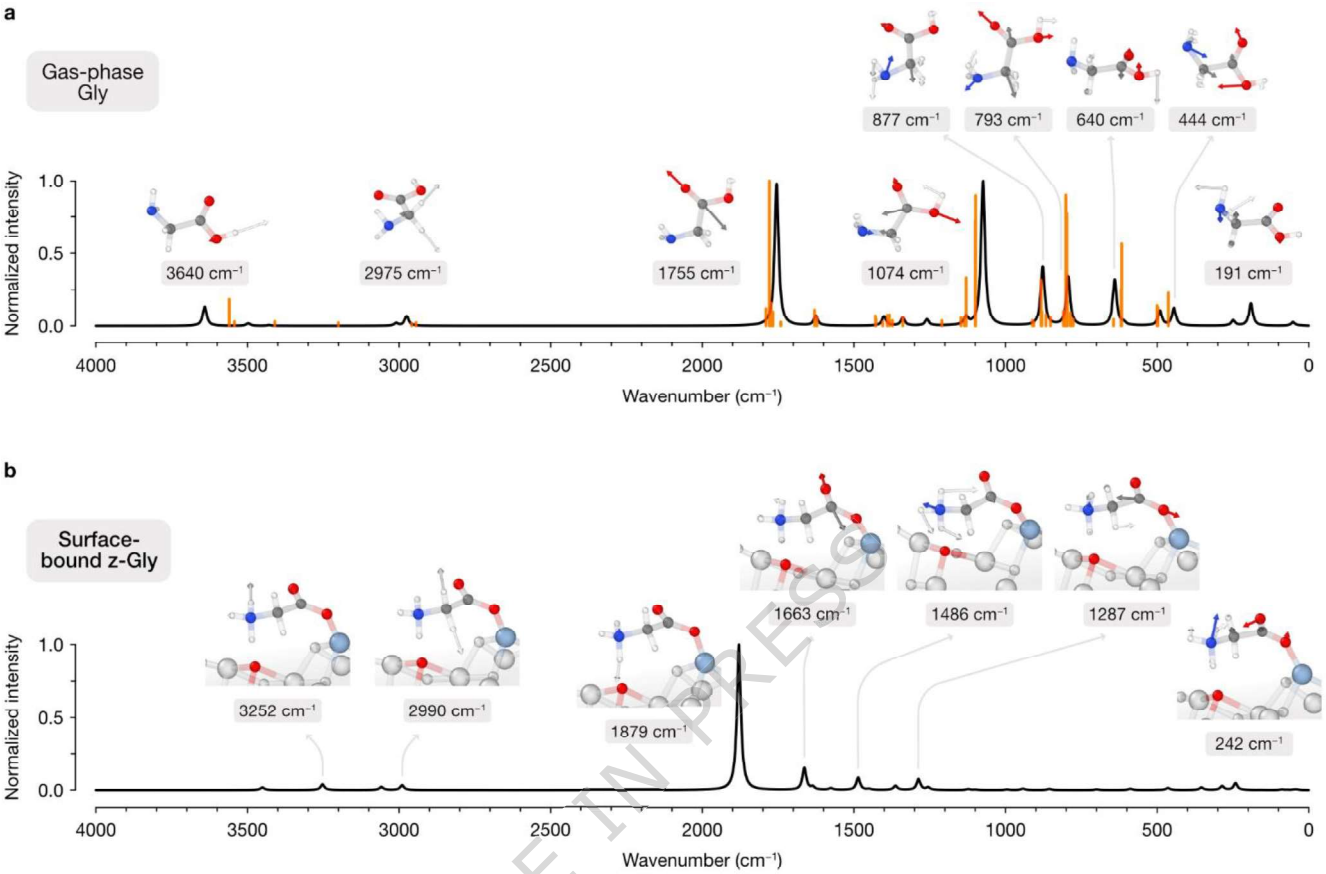

Figure 3. Spectral differentiation of Gly formed via the proposed direct pathway on Mg2SiO4. PBE-D3-simulated IR spectra of Gly formed through a conventional Strecker-based gas-phase mechanism (**a**), and of z-Gly* through the proposed mineral-mediated mechanism on $Mg_2SiO_4(021)$ (**b**). In **a**, the wavelengths and relative intensities of the IR peaks observed experimentally have been included as orange lines. Atomic representations of the features defining the peaks with the highest intensities are displayed as insets, where atomic displacements within a chosen direction of the vibrational mode are depicted as arrows with relative magnitudes. To aid visualization of vectors lying within atomic bonds, the latter are displayed in clear. Atoms from the surface in **b** that do not bind to z-Gly* (either through ionic or H-bonding) have been whitened out for clarity. Atom color codes can be found in Figures 1 and 2.

adopting an Eley–Rideal (ER) mechanism. While a Langmuir-Hinshelwood (LH) mechanism involving adsorbed CO was also considered, it was discarded on both energetic and steric grounds; CO chemisorption, which is less favorable than H_2CO adsorption by around 26 kcal mol^{-1}, occurs via the C atom, orienting the reactive center toward the surface and sterically preventing the C–C bond formation required for the reaction. In the proposed pathway, we predict the formation of an adsorbed acetolactone intermediate ($H_2C_2O_{2(cyc)}$*, the smallest member of the cyclic lactone family). This process presents an energy barrier of 38.19 kcal mol^{-1} in the gas-phase (mechanism displayed in Figure 2a), which decreases to 14.45 kcal mol^{-1} when taking place on the $Mg_2SiO_4(120)$ surface (gray pathway in Figure 2b). More importantly, the newly formed $H_2C_2O_{2(cyc)}$* intermediate, whose formation is only slightly endoergic (6.58 kcal mol^{-1} with respect to H_2CO*), displays a similar surface-induced charge redistribution as H_2CO*, and hence is able to react with gas-phase NH_3 in a barrierless fashion, followed

by spontaneous cleavage of the C-C bond to yield surface-bound zwitterionic Gly (z-Gly*) in a highly exoergic process. These results contrast with the gas-phase, where z-Gly is deemed unstable and formation of neutral Gly through the lactone-mediated pathway occurs following ammonolysis, with a larger energy barrier of 8.54 kcal mol^{-1}.

Additionally, although the adsorption of NH_3 onto a bare surface Mg site constitutes a potential energy well (being ~3 kcal mol^{-1} more stable than H_2CO*) that sequesters the N lone pair, we predict the reaction to proceed through the proposed route via an ER pathway because the subsequent steps are energetically decisive; once $H_2C_2O_{2(cyc)}$* is formed, our calculations predict its reaction with NH_3 to be vastly more exoergic than the competing adsorption of NH_3 onto a bare Mg site. Given that both ammonia capture processes are barrierless, the deep thermodynamic sink provided by Gly formation effectively drives the reaction forward, overcoming the slight initial stability of the adsorbed NH_3* over H_2CO*.

To further demonstrate the feasibility of the proposed pathway in other silicate terminations and extrapolate our results to predict the feasibility of this process on amorphous phases, we also investigated this reaction mechanism on a more energetic termination of Mg_2SiO_4, namely Mg_2SiO_4(021) (red pathway in Figure 2b). This facet, albeit displaying a higher surface energy with respect to Mg_2SiO_4(120), is still present in the equilibrium shape of Mg_2SiO_4 at 0 K with a coverage fraction of 0.047, thus potentially yielding multiple undercoordinated surface sites for reactant adsorption and reaction. Following the results on Mg_2SiO_4(120), H_2CO adsorbs on a surface Mg site of Mg_2SiO_4(021) to form H_2CO*, which in a similar process to the previously calculated pathway, reacts with gas-phase CO to form the $H_2C_2O_{2(cyc)}$* intermediate. This species subsequently reacts with gas-phase NH_3, again, in a barrierless way spontaneously yielding z-Gly* in a highly exoergic fashion. In this case, lactone formation on Mg_2SiO_4(021) displays a barrier of 9.98 kcal mol^{-1}, that is, 31 % lower than on Mg_2SiO_4(120), driven by the increased activity of the considered termination, and a striking 74 % lower than in the gas-phase mechanism. This single transition state for the formation of z-Gly results in a rate constant of 0.54 min^{-1} at 150 K, showcasing the feasibility of this pathway in the conditions found in interstellar ice-free warm environments such as hot-cores and protoplanetary disk regions where dust settles. Furthermore, the endergonic nature of $H_2C_2O_{2(cyc)}$* with respect to H_2CO* is reduced to 4.93 kcal mol^{-1}. Structural analysis of the $H_2C_2O_{2(cyc)}$* intermediates reveals that their stability is strongly influenced by their configuration on the mineral surface. On Mg_2SiO_4(120), steric hindrance and ionic repulsion with surface atoms constrain the intermediate to an upright orientation perpendicular to the surface, as shown in Figure S1. In contrast, the local environment of $H_2C_2O_{2(cyc)}$* on Mg_2SiO_4(021) accommodates the intermediate in a tilted configuration, allowing the carbonyl group to align more parallel to the surface. This favorable geometry enhances the stability of the intermediate ($\Delta G_{H_2C_2O_2^*}$ = 5.05 kcal mol^{-1} on Mg_2SiO_4(021) and 6.58 kcal mol^{-1} on Mg_2SiO_4(120)), which contributes to the observed decrease in the activation barrier for $H_2C_2O_{2(cyc)}$* formation on Mg_2SiO_4(021) compared to Mg_2SiO_4(120).

Interestingly, we predict that the formed z-Gly*, which is stabilized on surface Lewis acidic sites over its neutral counterpart,[57] displays high binding energies: 80.62 and 74.09 kcal mol^{-1} on Mg_2SiO_4(120) and Mg_2SiO_4(021), respectively. Therefore, our calculations show that, upon formation, z-Gly remains firmly embedded on the mineral surface and does not desorb thermally under the conditions of star forming regions. Specifically, an analysis of the non-

covalent interactions within the z-Gly* complex (Figure 2c) reveals that, in addition to the ionic interaction between the O atoms of the deprotonated carboxyl group and a surface Mg on $Mg_2SiO_4(120)$ and $Mg_2SiO_4(021)$, z-Gly* is also highly stabilized on the surface by means of H-bonding between the protonated amino group and a surface O atom (blue peaks of Figure 2c).

Finally, while our calculated energetics focus on a temperature of 150 K as a representative condition within warm regions of star formation, it is worth noting that the results gain further relevance at higher temperatures. As detailed in the Arrhenius plots provided in the Figure S2, the reaction rates for the mineral-mediated pathways increase by orders of magnitude as temperatures rise; this suggests that this mechanism remains efficient not only in warm star-forming regions but potentially also in hotter environments, such as the inner regions of protoplanetary disks or within asteroid parent bodies, where recent evidence points to aqueous chemistry.[58]

Spectral differentiation of surface-induced Gly. Building upon our prediction of the novel, energy-efficient mechanism on silicate surfaces, yielding the formation of z-Gly* over its neutral form, we hypothesize that this unique chemical environment can manifest in the vibrational properties of the newly-formed product. To investigate this, we computed the infra-red (IR) spectra of both gas-phase Gly and z-Gly* adsorbed on $Mg_2SiO_4(021)$. These calculations allow us to assess how surface binding affects the spectroscopic signature of Gly, and its impact on Gly detectability in astronomical environments. The computed gas-phase IR spectrum for the lowest-energy conformation of Gly (Figure 3a) exhibits the expected vibrational modes for this molecule, including the OH and CH stretching modes at high frequencies, followed by the isotopomer-determining mid- and low-frequency regions with C=O stretching at 1755 cm^{-1}, C–O and C–N stretching and COH bending modes around 1074 cm^{-1}, and low-energy modes of C–C stretching and CNH, CCO and COH bending at frequencies below 900 cm^{-1}. These peaks display an accurate match both in their location and intensity with reported experimental values in literature,[59] further validating our approach.

On the other hand, the vibrational spectrum of z-Gly* adsorbed on the silicate surface (Figure 3b) displays substantial differences, including shifts and even suppression of characteristic gas-phase modes. Notably, the strong interaction between the carboxylate COO^- group and the surface Mg centers, along with H-bonds between the NH_3^+ group and surface oxygen atoms, leads to pronounced alterations in both the position and intensity of key spectral features. Particularly, we note the suppression of the high-frequency features corresponding to the OH stretching and COH bending modes (due to the zwitterionic nature of z-Gly*), the slight blueshift of CH and CO stretching modes, and the emergence of multiple bands associated with NH stretching modes, particularly a high intensity peak corresponding to NH stretching along the highly directional H-bond at 1879 cm^{-1}. The absence of gas-phase fingerprints and appearance of new spectral features, albeit modulated by the local coordination environment, are predicted for z-Gly* adsorbed on both $Mg_2SiO_4(021)$ and $Mg_2SiO_4(120)$, both displaying the prevalence of a predicted peak corresponding to NH stretching along the highly directional H-bond (Figure S3). These results indicate distinct spectroscopic signatures for Gly formed through a mineral-mediated pathway, providing new vibrational markers that can guide future observational efforts, rather than relying onto gas-phase spectroscopic features, which have proven unfruitful for its detection.

Conclusions

In this work, we have explored, for the first time, the role of the parent body mineral surfaces in the abiotic formation of Gly at relatively warm stages of star-forming regions. By employing atomistic simulations based on quantum chemical calculations, we show that the conventional Strecker synthesis on abundant silicate surfaces (here modelled as crystalline Mg_2SiO_4), although facilitated by the grains, is hindered by high Gibbs energy barriers, rendering it inefficient under astrophysically relevant conditions, particularly due to the necessity of multiple water-mediated proton transfer steps. In contrast, we identify a direct pathway toward the formation of Gly from abundant zeroth-generation molecules (H_2CO, CO and NH_3) on Mg_2SiO_4, which proceeds without the involvement of high-energy radicals, ions, or water-mediated catalysis. This mechanism is enabled by surface-induced polarization effects that promote a spontaneous, barrierless process, culminating in the stable adsorption of zwitterionic Gly on the mineral surface via strong interactions. Furthermore, we show that surface terminations significantly impact the reaction kinetics, with Mg_2SiO_4(021) reducing the energy barrier for Gly formation by 74% compared to the gas-phase. After formation, we show that Gly is strongly attached to the surface and thus is unlikely to desorb even under hot-core temperatures. This presents a distinct survival advantage compared to Gly synthesized in cold, dense clouds: while ice-embedded molecules risk sublimation or destruction during the warm-up phase as the ice mantle evaporates, the Gly formed through the proposed mineral-mediated pathway may remain embedded on mineral grains and be incorporated into pebbles/planetesimal, cometary and meteoritic bodies. Finally, IR analyses reveal that the formed surface-bound Gly presents vastly distinct spectral features with respect to its gas-phase counterpart, providing a potential interpretation for the absence of observational evidence towards interstellar Gly in the gas-phase as well as guides for future identification.

Overall, our findings reveal a plausible, silicate-mediated low-energy pathway for Gly formation in warm star-forming environments that does not rely on energetic processing or aqueous chemistry. This supports the hypothesis that biologically relevant molecules may originate from solid-state reactions on mineral interfaces within early planetary systems, offering new insight into the origin of life's building blocks in space.

Methods

Simulation of gas-phase species. Reaction species involved in the studied gas phase mechanism were optimized using the PBE functional and the D3 Grimme's correction for dispersion, using Ahlrichs' def2-TZVP polarized triple-zeta basis set. Subsequently, single point energy calculations were performed using the Becke, 3-parameter, Lee–Yang–Parr (B3LYP),[60] PBE0[61] and range-separated screened Heyd–Scuseria–Ernzerhof (HSE06)[62,63] hybrid functionals with the same D3 approach and basis set, and comparing the relative energies with respect to those obtained using the explicitly correlated coupled-cluster variant coupled cluster theory with singles, doubles, and a perturbative treatment of triples (CCSD(T)-F12)[64] in conjunction with cc-pVTZ-F12 as the main basis set, including cc-pVTZ-F12-CABS, aug-cc-pVTZ, and aug-cc-pVQZ/C as auxiliary basis sets.[65] Gas phase simulations were performed using the ORCA package, version 5.0.3;[66] however, single-point calculations using the HSE06 functional were performed using the Gaussian16 software[67] with identical basis set to ensure a diverse landscape of hybrid functionals for an accurate benchmark. This benchmark yielded relative energies with mean absolute errors of 9.68, 6.29, 2.30 and 1.66 kcal mol^{-1} for PBE0-D3, PBE-D3, B3LYP-D3 and HSE06-D3, respectively relative to coupled-cluster calculations;

thus, all relative energies reported in this work correspond to single-point calculations of PBE-D3 optimizations at the HSE06-D3 level of theory.

Simulation of periodic systems. All periodic density functional theory calculations reported in this work were carried out using the Vienna Ab Initio Simulation package (VASP), version 6.4.[68] The Mg_2SiO_4 bulk, belonging to the *Pbnm* space group, was obtained from the Materials Project (id: mp-2895).[69] Periodic structure optimizations were performed using the PBE-D3 method[70,71] and the standard potentials based on the projector augmented-wave method[72] (treating the semi-core 2p electrons of Mg as valence electrons), with a plane wave energy cut-off of 500 eV Optimal lattice parameters were obtained by plotting the cell potential energy against varying cell volumes, modifying the cell size in a range of ±2% with a step size of 1%, using a Birch–Murnaghan equation of state while sampling the reciprocal space with increasing *k*-point grids of 2×2×1, 4×4×2, 8×6×4 and 12×10×6. Ultimately, a *k*-point grid of 4×4×2 was selected following a convergence criterion of 1 meV $atom^{-1}$, yielding cell parameters *a*, *b* and *c* of 4.779 Å, 6.017 Å and 10.271 Å, respectively. Subsequent structural optimizations of the periodic systems reported in this work were performed computing the corresponding *k*-point grids following the obtained optimal mean *k*-point density of around 3.4 *k*-points per $Å^{-1}$ in bulk optimization, using a conjugate-gradient scheme with a force-based convergence criterion of 0.015 eV/Å. According to benchmarking results in the gas phase (see above), single point calculations were performed onto the PBE-D3 optimized structures at the HSE06-D3 level at Γ-point implemented in VASP.

Non-polar (120) and (021) surface terminations of Mg_2SiO_4 in the *Pbnm* setting (corresponding to (102) and (012) in the standard *Pnma* space group, respectively), with an approximate thickness of 11 Å and a vacuum in the *c* axis of at least 15 Å, were generated with an in-house automated algorithm.[40] These surfaces, of which (120) is the most extended on the calculated equilibrium shape of Mg_2SiO_4, were selected based on their varying surface energies (1.41 and 1.92 J m^{-2} for (120) and (021), respectively[73]). The initial H_2CO adsorbate on the most stable active site of the (120) surface was obtained from previous work;[40] this adsorbate is deemed a global minimum on the surface, as recently validated by a pairwise potential-based approach,[74] and is an accurate representation of the most feasible surface site onto which H_2CO can adsorb and subsequently react. All adsorbate species were calculated using free-standing slabs with multiplicities *p*(2×1) for both (120) and (021) to ensure non-interaction between adsorbates in neighboring cells, where all atoms in the cell were allowed to relax freely. Minimum energy paths between intermediates were explored using the climbing image-nudged elastic band (CI-NEB) method[75,76] with 6 interpolated images using the force-based quick-min optimizer with a force-based convergence criterion of 0.02 eV/Å, as implemented in the VTST code. To ensure that all intermediates and transition state structures correspond to true minima and first order saddle points, respectively, a partial Hessian matrix was calculated using the finite differences method in all Cartesian coordinates, only computing the components of the matrix corresponding to the atoms participating in the reaction; in that regard, minima displaying negative frequencies had their atoms displaced along their imaginary vibrational mode and further optimized decreasing the minimum atomic displacement from 0.03 to 0.01 Å and using a denser FFT mesh. Similarly, saddle point candidates with more than one imaginary vibrational mode were fine-tuned using the dimer method[77] and a similar convergence criterion. All reported energies in the mechanisms presented herein are relative to the bare surface and the corresponding

species in the gas phase, which for this purpose, were optimized in a periodic cell ensuring a 15 Å vacuum in all Cartesian coordinates.

Gibbs energy corrections computed at PBE-D3, which include the zero-point energy, entropy and thermal contributions to the internal energy, were added to the HSE06-D3 energy of all species using the harmonic limit approach implemented in the Atomic Simulation Environment (ASE) package.[78] All Gibbs energy values reported in the potential energy surfaces shown in this work are calculated at a temperature of 150 K, characteristic of warm up regions of star formation.

Charge density differences between the surface and the H_2CO adsorbate were computed by subtracting the charge of the isolated adsorbate and bare surface from the adsorbate-surface system in their optimized configurations, and subsequently averaged and plotted along the z axis using the SISL software.[79] Non-covalent interactions (NCIs) of relevant structures were revealed by computing NCI plots showing the interactions between the adsorbates and the surface sites, as implemented in the Critic2 software[80] (we direct the reader to relevant literature on this matter).[81,82] We note that NCI plots provide a pseudo-quantitative representation of all non-covalent interactions governing the stabilization of the molecule on the surface, where the more negative (positive) the peaks appear, the more attractive (repulsive) that specific interaction is.

For the proposed direct pathway, which follows an Eley-Rideal mechanism, the reaction rate r is formally described as

$$r = k\theta_{H_2CO}[CO]$$

Where k is the rate constant, θ_{H_2CO} is the fractional surface coverage of formaldehyde, and $[CO]$ is the concentration of gas-phase CO. Given the nature of the modelled systems and proposed mechanisms, values for k are calculated using the classical Eyring equation,

$$k = \frac{k_B T}{h} e^{-\frac{\Delta G^{\ddagger}}{RT}}$$

where $\Delta G^{\ddagger}$ is the Gibbs energy barrier for the rate limiting step, T is the considered temperature, and R, k_B and h are the ideal gas, Boltzmann and Planck constants, respectively. In contrast to the values reported in Figures 1a and 2b, activation energies considered in the Arrhenius plots were calculated dynamically at each temperature step; resulting rates were plotted as $\log_{10}(k)$ against the inverse of the temperature.

IR spectra of gas-phase Gly and z-Gly* were constructed by computing vibrational frequencies and Born effective charges at Γ-point using density functional perturbation theory (DFPT). Vibrational intensities were calculated as described by Gianozzi and Baroni[83] and implemented elsewhere.[44]

Acknowledgements

This project is part of the grant no. JDC2023-051088-I, funded by the MCIU/AEI/10.13039/501100011033 and the FSE+ fund. This project also received funding from the European Research Council (ERC) under the European Union's Horizon 2020 Research and Innovation Program (Grant Agreement 865657) for Project "Quantum Chemistry on Interstellar Grains" (QUANTUMGRAIN). MICIN is also acknowledged for financing the projects PID2021-126427NBI00 and CNS2023-144902. A. R. acknowledges Accademia delle Scienze di Torino for supporting the project "In silico interstellar grain-surface chemistry". A. R. gratefully acknowledges support through a 2023 ICREA Award. We acknowledge the provision of computational resources by CSUC and the EuroHPC Joint Undertaking through project no. 2023R01-112, hosted by the Ministry of Education, Youth and

Sports of the Czech Republic through the e-INFRA CZ (ID: 9025).

Author contributions

E. M.-T. conceptualized the study, performed the calculations, analyzed the results, and wrote the manuscript with input from A. R. A. R. supervised the study, secured the funding and provided the research infrastructure.

Data availability

Input and output files of all the calculations reported in this work can be accesses via an ioChem-BD database with the following DOI: 10.19061/iochem-bd-6-572.

Competing interests

The authors declare no competing interests.

References

1. Martins, Z., Alexander, C. M. O., Orzechowska, G. E., Fogel, M. L. & Ehrenfreund, P. Indigenous amino acids in primitive CR meteorites. *Meteorit. Planet. Sci.* **42**, 2125–2136 (2007).
2. Kvenvolden, K., Lawless, J., Pering, K., Peterson, E., Flores, J., Ponnamperuma, C., Kaplan, I. R. & Moore, C. Evidence for Extraterrestrial Amino-acids and Hydrocarbons in the Murchison Meteorite. *Nature* **228**, 923–926 (1970).
3. Potiszil, C., Ota, T., Yamanaka, M., Sakaguchi, C., Kobayashi, K., Tanaka, R., Kunihiro, T., Kitagawa, H., Abe, M., Miyazaki, A., Nakato, A., Nakazawa, S., Nishimura, M., Okada, T., Saiki, T., Tanaka, S., Terui, F., Tsuda, Y., Usui, T., Watanabe, S., Yada, T., Yogata, K., Yoshikawa, M. & Nakamura, E. Insights into the formation and evolution of extraterrestrial amino acids from the asteroid Ryugu. *Nat. Commun.* **14**, 1482 (2023).
4. Elsila, J. E., Glavin, D. P. & Dworkin, J. P. Cometary glycine detected in samples returned by Stardust. *Meteorit. Planet. Sci.* **44**, 1323–1330 (2009).
5. Glavin, D. P., Dworkin, J. P. & Sandford, S. A. Detection of cometary amines in samples returned by Stardust. *Meteorit. Planet. Sci.* **43**, 399–413 (2008).
6. Altwegg, K., Balsiger, H., Bar-Nun, A., Berthelier, J.-J., Bieler, A., Bochsler, P., Briois, C., Calmonte, U., Combi, M. R., Cottin, H., De Keyser, J., Dhooghe, F., Fiethe, B., Fuselier, S. A., Gasc, S., Gombosi, T. I., Hansen, K. C., Haessig, M., Jäckel, A., Kopp, E., Korth, A., Le Roy, L., Mall, U., Marty, B., Mousis, O., Owen, T., Rème, H., Rubin, M., Sémon, T., Tzou, C.-Y., Hunter Waite, J. & Wurz, P. Prebiotic chemicals—amino acid and phosphorus—in the coma of comet 67P/Churyumov-Gerasimenko. *Sci. Adv.* **2**, e1600285 (2016).
7. Kuan, Y., Charnley, S. B., Huang, H., Tseng, W. & Kisiel, Z. Interstellar Glycine. *Astrophys. J.* **593**, 848–867 (2003).
8. Snyder, L. E., Lovas, F. J., Hollis, J. M., Friedel, D. N., Jewell, P. R., Remijan, A., Ilyushin, V. V., Alekseev, E. A. & Dyubko, S. F. A Rigorous Attempt to Verify Interstellar Glycine. *Astrophys. J.* **619**, 914–930 (2005).
9. Carl, T., Wirström, E. S., Bergman, P., Charnley, S. B., Chuang, Y.-L. & Kuan, Y.-J. Deep search for glycine conformers in Barnard 5. *Mon. Not. R. Astron. Soc.* **524**, 5993–6003 (2023).
10. Lattelais, M., Pauzat, F., Pilmé, J., Ellinger, Y. & Ceccarelli, C. About the detectability of glycine in the interstellar medium. *Astron. Astrophys.* **532**, A39 (2011).
11. Rivilla, V. M., Sanz-Novo, M., Jiménez-Serra, I., Martín-Pintado, J., Colzi, L., Zeng, S., Megías,

A., López-Gallifa, Á., Martínez-Henares, A., Massalkhi, S., Tercero, B., De Vicente, P., Martín, S., Andrés, D. S., Requena-Torres, M. A. & Alonso, J. L. First Glycine Isomer Detected in the Interstellar Medium: Glycolamide (NH_2 $C(O)CH_2$ OH). *Astrophys. J. Lett.* **953**, L20 (2023).

12. Hollis, J. M., Snyder, L. E., Suenram, R. D. & Lovas, F. J. A search for the lowest-energy conformer of interstellar glycine. *Astrophys. J.* **241**, 1001 (1980).
13. Ceccarelli, C., Loinard, L., Castets, A., Faure, A. & Lefloch, B. Search for glycine in the solar type protostar IRAS 16293-2422. *Astron. Astrophys.* **362**, 1122–1126 (2000).
14. Jiménez-Serra, I., Testi, L., Caselli, P. & Viti, S. DETECTABILITY OF GLYCINE IN SOLAR-TYPE SYSTEM PRECURSORS. *Astrophys. J.* **787**, L33 (2014).
15. Bockelée-Morvan, D. & Biver, N. The composition of cometary ices. *Philos. Trans. R. Soc. Math. Phys. Eng. Sci.* **375**, 20160252 (2017).
16. Jørgensen, J. K., Belloche, A. & Garrod, R. T. Astrochemistry During the Formation of Stars. *Annu. Rev. Astron. Astrophys.* **58**, 727–778 (2020).
17. Herbst, E. & van Dishoeck, E. F. Complex Organic Interstellar Molecules. *Annu. Rev. Astron. Astrophys.* **47**, 427–480 (2009).
18. Van Dishoeck, E. F. & Blake, G. A. CHEMICAL EVOLUTION OF STAR-FORMING REGIONS. *Annu. Rev. Astron. Astrophys.* **36**, 317–368 (1998).
19. Theulé, P., Duvernay, F., Danger, G., Borget, F., Bossa, J. B., Vinogradoff, V., Mispelaer, F. & Chiavassa, T. Thermal reactions in interstellar ice: A step towards molecular complexity in the interstellar medium. *Adv. Space Res.* **52**, 1567–1579 (2013).
20. Garrod, R. T., Weaver, S. L. W. & Herbst, E. Complex Chemistry in Star-forming Regions: An Expanded Gas-Grain Warm-up Chemical Model. *Astrophys. J.* **682**, 283–302 (2008).
21. Thripati, S. Computational studies on the possible formation of glycine *via* open shell gas-phase chemistry in the interstellar medium. *Org. Biomol. Chem.* **20**, 4189–4203 (2022).
22. Choe, J. C. Mechanisms of glycine formation from aminoacetonitrile in space. *Phys. Chem. Chem. Phys.* **25**, 16001–16008 (2023).
23. Maeda, S. & Ohno, K. Ab initio Studies on Synthetic Routes of Glycine from Simple Molecules via Ammonolysis of Acetolactone: Applications of the Scaled Hypersphere Search Method. *Chem. Lett.* **33**, 1372–1373 (2004).
24. Krasnokutski, S. A., Jäger, C. & Henning, T. Condensation of Atomic Carbon: Possible Routes toward Glycine. *Astrophys. J.* **889**, 67 (2020).
25. Largo, L., Redondo, P., Rayón, V. M., Largo, A. & Barrientos, C. The reaction between NH_3^+ and CH_3 COOH: a possible process for the formation of glycine precursors in the interstellar medium. *Astron. Astrophys.* **516**, A79 (2010).
26. Maeda, S. & Ohno, K. Generation Mechanisms of Amino Acids in Interstellar Space via Reactions between Closed-Shell Species: Significance of Higher Energy Isomers in Molecular Evolution. *Astrophys. J.* **640**, 823–828 (2006).
27. Maeda, S. & Ohno, K. No activation barrier synthetic route of glycine from simple molecules (NH_3, CH_2, and CO_2) via carboxylation of ammonium ylide: a theoretical study by the scaled hypersphere search method. *Chem. Phys. Lett.* **398**, 240–244 (2004).
28. Redondo, P., Largo, A. & Barrientos, C. Is the reaction between formic acid and protonated aminomethanol a possible source of glycine

precursors in the interstellar medium? *Astron. Astrophys.* **579**, A125 (2015).

29. Zhu, H.-S. & Ho, J.-J. Ab Initio Study of the Formation of Glycine via Amino Acetonitrile and Amino-Cyano-Acetic Acid. *J. Phys. Chem. A* **108**, 3798–3805 (2004).

30. Huet, L., Devergne, T., Magrino, T. & Saitta, A. M. A New Route to the Prebiotic Synthesis of Glycine via *Ab Initio* -Based Machine Learning Calculations. *J. Phys. Chem. Lett.* **15**, 8697–8705 (2024).

31. Nhlabatsi, Z. P., Bhasi, P. & Sitha, S. Possible interstellar formation of glycine through a concerted mechanism: a computational study on the reaction of CH_2=NH, CO_2 and H_2. *Phys. Chem. Chem. Phys.* **18**, 20109–20117 (2016).

32. Lee, H. M. & Choe, J. C. Formation of glycine from HCN and H_2O: A computational mechanistic study. *Chem. Phys. Lett.* **675**, 6–10 (2017).

33. Koch, D. M., Toubin, C., Peslherbe, G. H. & Hynes, J. T. A Theoretical Study of the Formation of the Aminoacetonitrile Precursor of Glycine on Icy Grain Mantles in the Interstellar Medium. *J. Phys. Chem. C* **112**, 2972–2980 (2008).

34. Magrino, T., Pietrucci, F. & Saitta, A. M. Step by Step Strecker Amino Acid Synthesis from Ab Initio Prebiotic Chemistry. *J. Phys. Chem. Lett.* **12**, 2630–2637 (2021).

35. Woon, D. E. Pathways to Glycine and Other Amino Acids in Ultraviolet-irradiated Astrophysical Ices Determined via Quantum Chemical Modeling. *Astrophys. J.* **571**, L177–L180 (2002).

36. Rimola, A., Sodupe, M. & Ugliengo, P. COMPUTATIONAL STUDY OF INTERSTELLAR GLYCINE FORMATION OCCURRING AT RADICAL SURFACES OF WATER-ICE DUST PARTICLES. *Astrophys. J.* **754**, 24 (2012).

37. Carrascoza, F., Lukasiak, P., Nowak, W. & Blazewicz, J. Ab Initio Study of Glycine Formation in the Condensed Phase: Carbon Monoxide, Formaldimine, and Water Are Enough. *Astrophys. J.* **956**, 140 (2023).

38. Rimola, A., Sodupe, M. & Ugliengo, P. Deep-space glycine formation via Strecker-type reactions activated by ice water dust mantles. A computational approach. *Phys. Chem. Chem. Phys.* **12**, 5285 (2010).

39. Ioppolo, S., Fedoseev, G., Chuang, K.-J., Cuppen, H. M., Clements, A. R., Jin, M., Garrod, R. T., Qasim, D., Kofman, V., Van Dishoeck, E. F. & Linnartz, H. A non-energetic mechanism for glycine formation in the interstellar medium. *Nat. Astron.* **5**, 197–205 (2020).

40. Mates-Torres, E. & Rimola, A. Unlocking the surface chemistry of ionic minerals: a high-throughput pipeline for modeling realistic interfaces. *J. Appl. Crystallogr.* **57**, 503–508 (2024).

41. Bancone, N., Pantaleone, S., Ugliengo, P., Rimola, A. & Corno, M. Adsorption of HCN on cosmic silicates: a periodic quantum mechanical study. *Phys. Chem. Chem. Phys.* **25**, 26797–26812 (2023).

42. Bancone, N., Santalucia, R., Pantaleone, S., Ugliengo, P., Mino, L., Rimola, A. & Corno, M. Unraveling the Interface Chemistry between HCN and Cosmic Silicates by the Interplay of Infrared Spectroscopy and Quantum Chemical Modeling. *J. Phys. Chem. C* **128**, 15171–15178 (2024).

43. Perrero, J., Beitia-Antero, L., Fuente, A., Ugliengo, P. & Rimola, A. Theoretical modelling of the adsorption of neutral and charged sulphur-bearing species on to olivine nanoclusters. *Mon. Not. R. Astron. Soc.* **527**, 10697–10704 (2023).

44.Mates-Torres, E., Escolano Casado, G., Mino, L., Balucani, N., Ugliengo, P. & Rimola, A. Revealing SO_2 and CO_2 adsorption features on forsterite *via* IR spectroscopy and automated computational approaches. *Phys. Chem. Chem. Phys.* **27**, 13124–13134 (2025).

45.Rubin, A. E. Mineralogy of meteorite groups. *Meteorit. Planet. Sci.* **32**, 231–247 (1997).

46.Ishii, H. A., Bradley, J. P., Dai, Z. R., Chi, M., Kearsley, A. T., Burchell, M. J., Browning, N. D. & Molster, F. Comparison of Comet 81P/Wild 2 Dust with Interplanetary Dust from Comets. *Science* **319**, 447–450 (2008).

47.Lambert, J. B., Gurusamy-Thangavelu, S. A. & Ma, K. The Silicate-Mediated Formose Reaction: Bottom-Up Synthesis of Sugar Silicates. *Science* **327**, 984–986 (2010).

48.Vinogradoff, V., Leyva, V., Mates-Torres, E., Pepino, R., Danger, G., Rimola, A., Cazals, L., Serra, C., Pascal, R. & Meinert, C. Olivine-catalyzed glycolaldehyde and sugar synthesis under aqueous conditions: Application to prebiotic chemistry. *Earth Planet. Sci. Lett.* **626**, 118558 (2024).

49.Bancone, N., Pantaleone, S., Ugliengo, P., Rimola, A. & Corno, M. Exploring Forsterite Surface Catalysis in HCN Polymerization: Computational Insights for Astrobiology and Prebiotic Chemistry. *ACS Earth Space Chem.* **9**, 303–313 (2025).

50.Rimola, A., Balucani, N., Ceccarelli, C. & Ugliengo, P. Tracing the Primordial Chemical Life of Glycine: A Review from Quantum Chemical Simulations. *Int. J. Mol. Sci.* **23**, 4252 (2022).

51.Aponte, J. C., Elsila, J. E., Glavin, D. P., Milam, S. N., Charnley, S. B. & Dworkin, J. P. Pathways to Meteoritic Glycine and Methylamine. *ACS Earth Space Chem.* **1**, 3–13 (2017).

52.Godfrey, P. D., Brown, R. D., Robinson, B. J. & Sinclair, M. W. Discovery of Interstellar Methanimine (Formaldimine). *Astrophys. Lett.* **13**, 119 (1973).

53.San Andrés, D., Rivilla, V. M., Colzi, L., Jiménez-Serra, I., Martín-Pintado, J., Megías, A., López-Gallifa, Á., Martínez-Henares, A., Massalkhi, S., Zeng, S., Sanz-Novo, M., Tercero, B., De Vicente, P., Martín, S., Requena Torres, M. A., Molpeceres, G. & García De La Concepción, J. First Detection in Space of the High-energy Isomer of Cyanomethanimine: H_2 CNCN. *Astrophys. J.* **967**, 39 (2024).

54.Rivilla, V. M., Martín-Pintado, J., Jiménez-Serra, I., Zeng, S., Martín, S., Armijos-Abendaño, J., Requena-Torres, M. A., Aladro, R. & Riquelme, D. Abundant Z-cyanomethanimine in the interstellar medium: paving the way to the synthesis of adenine. *Mon. Not. R. Astron. Soc. Lett.* **483**, L114–L119 (2019).

55.Molpeceres, G., Tsuge, M., Furuya, K., Watanabe, N., San Andrés, D., Rivilla, V. M., Colzi, L. & Aikawa, Y. Carbon Atom Condensation on NH_3 –H_2 O Ices. An Alternative Pathway to Interstellar Methanimine and Methylamine. *J. Phys. Chem. A* **128**, 3874–3889 (2024).

56.Bovolenta, G. M., Silva-Vera, G., Bovino, S., Molpeceres, G., Kästner, J. & Vogt-Geisse, S. In-depth exploration of catalytic sites on amorphous solid water: I. The astrosynthesis of aminomethanol. *Phys. Chem. Chem. Phys.* **26**, 18692–18706 (2024).

57.Yang, G. & Zhou, L. Zwitterionic versus canonical amino acids over the various defects in zeolites: A two-layer ONIOM calculation. *Sci. Rep.* **4**, 6594 (2014).

58.McCoy, T. J., Russell, S. S., Zega, T. J., Thomas-Keprta, K. L., Singerling, S. A., Brenker, F. E., Timms, N. E., Rickard, W. D. A., Barnes, J. J., Libourel, G., Ray, S., Corrigan, C. M.,

Haenecour, P., Gainsforth, Z., Dominguez, G., King, A. J., Keller, L. P., Thompson, M. S., Sandford, S. A., Jones, R. H., Yurimoto, H., Righter, K., Eckley, S. A., Bland, P. A., Marcus, M. A., DellaGiustina, D. N., Ireland, T. R., Almeida, N. V., Harrison, C. S., Bates, H. C., Schofield, P. F., Seifert, L. B., Sakamoto, N., Kawasaki, N., Jourdan, F., Reddy, S. M., Saxey, D. W., Ong, I. J., Prince, B. S., Ishimaru, K., Smith, L. R., Benner, M. C., Kerrison, N. A., Portail, M., Guigoz, V., Zanetta, P.-M., Wardell, L. R., Gooding, T., Rose, T. R., Salge, T., Le, L., Tu, V. M., Zeszut, Z., Mayers, C., Sun, X., Hill, D. H., Lunning, N. G., Hamilton, V. E., Glavin, D. P., Dworkin, J. P., Kaplan, H. H., Franchi, I. A., Tait, K. T., Tachibana, S., Connolly, H. C. & Lauretta, D. S. An evaporite sequence from ancient brine recorded in Bennu samples. *Nature* **637**, 1072–1077 (2025).

59. Stepanian, S. G., Reva, I. D., Radchenko, E. D., Rosado, M. T. S., Duarte, M. L. T. S., Fausto, R. & Adamowicz, L. Matrix-Isolation Infrared and Theoretical Studies of the Glycine Conformers. *J. Phys. Chem. A* **102**, 1041–1054 (1998).

60. Becke, A. D. Density-functional thermochemistry. III. The role of exact exchange. *J. Chem. Phys.* **98**, 5648–5652 (1993).

61. Adamo, C. & Barone, V. Toward reliable density functional methods without adjustable parameters: The PBE0 model. *J. Chem. Phys.* **110**, 6158–6170 (1999).

62. Heyd, J., Scuseria, G. E. & Ernzerhof, M. Hybrid functionals based on a screened Coulomb potential. *J. Chem. Phys.* **118**, 8207–8215 (2003).

63. Heyd, J., Scuseria, G. E. & Ernzerhof, M. Erratum: "Hybrid functionals based on a screened Coulomb potential" [J. Chem. Phys. 118, 8207 (2003)]. *J. Chem. Phys.* **124**, 219906 (2006).

64. Adler, T. B., Knizia, G. & Werner, H.-J. A simple and efficient CCSD(T)-F12 approximation. *J. Chem. Phys.* **127**, 221106 (2007).

65. Sylvetsky, N., Kesharwani, M. K. & Martin, J. M. L. The aug-cc-pVnZ-F12 basis set family: Correlation consistent basis sets for explicitly correlated benchmark calculations on anions and noncovalent complexes. *J. Chem. Phys.* **147**, 134106 (2017).

66. Neese, F., Wennmohs, F., Becker, U. & Riplinger, C. The ORCA quantum chemistry program package. *J. Chem. Phys.* **152**, 224108 (2020).

67. Frisch, M. J., Trucks, G. W., Schlegel, H. B., Scuseria, G. E., Robb, M. A., Cheeseman, J. R., Scalmani, G., Barone, V., Petersson, G. A., Nakatsuji, H., Li, X., Caricato, M., Marenich, A. V., Bloino, J., Janesko, B. G., Gomperts, R., Mennucci, B., Hratchian, H. P., Ortiz, J. V., Izmaylov, A. F., Sonnenberg, J. L., Williams-Young, D., Ding, F., Lipparini, F., Egidi, F., Goings, J., Peng, B., Petrone, A., Henderson, T., Ranasinghe, D., Zakrzewski, V. G., Gao, J., Rega, N., Zheng, G., Liang, W., Hada, M., Ehara, M., Toyota, K., Fukuda, R., Hasegawa, J., Ishida, M., Nakajima, T., Honda, Y., Kitao, O., Nakai, H., Vreven, T., Throssell, K., Montgomery, J. A., Jr., Peralta, J. E., Ogliaro, F., Bearpark, M. J., Heyd, J. J., Brothers, E. N., Kudin, K. N., Staroverov, V. N., Keith, T. A., Kobayashi, R., Normand, J., Raghavachari, K., Rendell, A. P., Burant, J. C., Iyengar, S. S., Tomasi, J., Cossi, M., Millam, J. M., Klene, M., Adamo, C., Cammi, R., Ochterski, J. W., Martin, R. L., Morokuma, K., Farkas, O., Foresman, J. B. & Fox, D. J. Gaussian 16, Revision B.01. (2016).

68. Kresse, G. & Furthmüller, J. Efficient iterative schemes for *ab initio* total-energy calculations using a plane-wave basis set. *Phys. Rev. B* **54**, 11169–11186 (1996).

69.Jain, A., Ong, S. P., Hautier, G., Chen, W., Richards, W. D., Dacek, S., Cholia, S., Gunter, D., Skinner, D., Ceder, G. & Persson, K. A. The Materials Project: A materials genome approach to accelerating materials innovation. *APL Mater.* **1**, 011002 (2013).

70.Perdew, J. P., Burke, K. & Ernzerhof, M. Generalized Gradient Approximation Made Simple. *Phys. Rev. Lett.* **77**, 3865–3868 (1996).

71.Grimme, S., Antony, J., Ehrlich, S. & Krieg, H. A consistent and accurate *ab initio* parametrization of density functional dispersion correction (DFT-D) for the 94 elements H-Pu. *J. Chem. Phys.* **132**, 154104 (2010).

72.Blöchl, P. E. Projector augmented-wave method. *Phys. Rev. B* **50**, 17953–17979 (1994).

73.Bruno, M., Massaro, F. R., Prencipe, M., Demichelis, R., De La Pierre, M. & Nestola, F. Ab Initio Calculations of the Main Crystal Surfaces of Forsterite (Mg_2SiO_4): A Preliminary Study to Understand the Nature of Geochemical Processes at the Olivine Interface. *J. Phys. Chem. C* **118**, 2498–2506 (2014).

74.Mates-Torres, E., Ugliengo, P. & Rimola, A. Mapping adsorption on ionic surfaces via a pairwise potential-based high-throughput approach. *J. Appl. Crystallogr.* **58**, (2025).

75.Jónsson, H., Mills, G. & Jacobsen, K. W. Nudged elastic band method for finding minimum energy paths of transitions. in *Classical and Quantum Dynamics in Condensed Phase Simulations* 385–404 (WORLD SCIENTIFIC, LERICI, Villa Marigola, 1998). doi:10.1142/9789812839664_0016.

76.Henkelman, G., Uberuaga, B. P. & Jónsson, H. A climbing image nudged elastic band method for finding saddle points and minimum energy paths. *J. Chem. Phys.* **113**, 9901–9904 (2000).

77.Henkelman, G. & Jónsson, H. A dimer method for finding saddle points on high dimensional potential surfaces using only first derivatives. *J. Chem. Phys.* **111**, 7010–7022 (1999).

78.Hjorth Larsen, A., Jørgen Mortensen, J., Blomqvist, J., Castelli, I. E., Christensen, R., Dułak, M., Friis, J., Groves, M. N., Hammer, B., Hargus, C., Hermes, E. D., Jennings, P. C., Bjerre Jensen, P., Kermode, J., Kitchin, J. R., Leonhard Kolsbjerg, E., Kubal, J., Kaasbjerg, K., Lysgaard, S., Bergmann Maronsson, J., Maxson, T., Olsen, T., Pastewka, L., Peterson, A., Rostgaard, C., Schiøtz, J., Schütt, O., Strange, M., Thygesen, K. S., Vegge, T., Vilhelmsen, L., Walter, M., Zeng, Z. & Jacobsen, K. W. The atomic simulation environment—a Python library for working with atoms. *J. Phys. Condens. Matter* **29**, 273002 (2017).

79.Papior, N. & Febrer Calabozo, P. sisl. Zenodo https://doi.org/10.5281/ZENODO.597181 (2025).

80.Otero-de-la-Roza, A., Johnson, E. R. & Luaña, V. Critic2: A program for real-space analysis of quantum chemical interactions in solids. *Comput. Phys. Commun.* **185**, 1007–1018 (2014).

81.Contreras-García, J., Boto, R. A., Izquierdo-Ruiz, F., Reva, I., Woller, T. & Alonso, M. A benchmark for the non-covalent interaction (NCI) index or… is it really all in the geometry? *Theor. Chem. Acc.* **135**, (2016).

82.Contreras-García, J., Johnson, E. R., Keinan, S., Chaudret, R., Piquemal, J.-P., Beratan, D. N. & Yang, W. NCIPLOT: A Program for Plotting Noncovalent Interaction Regions. *J. Chem. Theory Comput.* **7**, 625–632 (2011).

83.Baroni, S., De Gironcoli, S., Dal Corso, A. & Giannozzi, P. Phonons and related crystal properties from density-functional perturbation theory. *Rev. Mod. Phys.* **73**, 515–562 (2001).

Editor's Summary

Glycine has been identified in several extraterrestrial environments, however, its detection in the interstellar medium remains elusive. Here, the authors investigate a catalytic pathway for glycine formation on silicate grains during relatively warm (>150 K) stages of star formation using atomistic simulations, proposing a mechanism involving low-energy surface-stabilized intermediates that lead to spontaneous formation of glycine in a single-barrier exoergic process.

Peer review information:

Communications Chemistry thanks the anonymous reviewers for their contribution to the peer review of this work. A peer review file is available.